

Hierarchical Refinement of Universal Multimodal Attacks on Vision-Language Models

Peng-Fei Zhang and Zi Huang

Abstract—Adversarial attacks, which apply imperceptible perturbations to mislead model predictions, are essential for evaluating the robustness of Vision-Language Pre-trained (VLP) models. However, existing adversarial attacks for VLP models are mostly sample-specific, resulting in substantial computational overhead when scaled to large datasets or new scenarios.

To overcome this limitation, we propose Hierarchical Refinement Attack (HRA), a multimodal universal attack framework for VLP models. HRA refines universal adversarial perturbations (UAPs) at both the sample level and the optimization level, improving transferability to effectively break cross-modal alignment across models, datasets and tasks. For the image modality, we disentangle adversarial examples into clean images and perturbations, allowing each component to be handled independently for more effective disruption of cross-modal alignment. We further introduce a ScMix augmentation strategy that diversifies visual contexts and strengthens both global and local utility of UAPs, thereby reducing reliance on spurious features. In addition, we refine the optimization path by leveraging a temporal hierarchy of historical and estimated future gradients to avoid local minima and stabilize universal perturbation learning. For the text modality, HRA identifies globally influential words by combining intra-sentence and inter-sentence importance measures, and subsequently utilizes these words as universal text perturbations. Extensive experiments across various downstream tasks, VLP models, and datasets, including cross-modal retrieval scenarios, visual grounding and other downstream tasks, demonstrate the superiority of the proposed universal multimodal attacks.

Index Terms—Vision-Language Models; Universal Adversarial Perturbations; Multi-modal Attacks; Adversarial Transferability.

I. INTRODUCTION

Vision-Language Pre-trained (VLP) models play a crucial role in bridging the gap between images and texts, enabling multimodal understanding, generation, and response. These models take advantage of abundant information from large-scale unlabelled datasets via self-supervised pre-training, e.g., CLIP [1], ALBEF [2], and TCL [3]. The knowledge acquired during the pre-training phase can be effectively transferred to various downstream tasks with minimal additional training, e.g., fine-tuning. This transferability makes VLP models highly versatile and efficient, allowing them to adapt to new tasks and datasets with relatively low computational costs. Due to their promising performance, VLP models have been widely applied to various vision-language tasks, ranging from multimodal retrieval [4] to image captioning [5].

As the deployment of VLP models continues to grow, evaluating their robustness has become essential. This is vitally

Peng-Fei Zhang, Zi Huang are with the School of Information Technology & Electrical Engineering, the University of Queensland, email: mima.zpf@gmail.com and huang@itee.uq.edu.au

important for real-world applications, especially in sensitive and high-stakes applications, where potential threats and uncertainties demand models that are both robust and reliable. Furthermore, uncovering model vulnerabilities would drive advancements in the development of more resilient and reliable neural networks. Adversarial attacks serve as one of the most critical strategies for assessing model vulnerabilities and have been widely studied and applied [6], [7], [8], [9], [10], [11], [12]. These attacks primarily involve crafting imperceptible perturbations that, when injected into data, can mislead models into making incorrect predictions.

Adversarial attacks were originally designed for unimodal scenarios, where only a single data modality is considered [6], [13], [8]. Recently, several studies have begun exploring specific multimodal tasks, e.g., image-text retrieval [14], [15], and visual question answering [16]. These methods typically rely on task-specific losses or model outputs and thus are not directly applicable to VLP models. For example, Zhang *et al.* [14], [15] propose to learn adversarial perturbations by enlarging the similarity between clean and adversarial data guided by a similarity matrix. Yin *et al.* [16] introduce a masked answer anti-recovery to prevent models from recovering the correct answer tokens for each masked text. Current methods for VLP attacks mainly concentrate on features that are independent of specific tasks and output, i.e., enlarging the feature distance between adversarial data and original data to break the cross-modal alignments [17]. Further, Lu *et al.* [18], [12] increase data diversity to better exploit cross-modal interactions, thereby promoting the transferability of perturbations. However, these methods customize adversarial perturbations for each sample based on specific characteristics of each sample. Sample-wise approaches have to learn adversarial perturbations for new data from scratch, resulting in significant computational overhead. This would significantly deter their applications from large-scale cases. Zhou *et al.* [19], [20] make early attempts to learn universal adversarial attacks for the image modality. However, the method in [19] is restricted to specific models, and neither work exploits text-based attacks, which could further enhance adversarial effectiveness. Fang *et al.* [21] consider both image and text universal attacks, where the text-side attacks are implemented through word substitutions. These substitutions are obtained by first learning adversarial embeddings and then searching the corpus for words that are semantically aligned with these embeddings. However, this method requires access to a predefined word library, and the mismatch between the learned adversarial embeddings and their final token-level realizations can weaken the attack effectiveness. In addition, these methods do not

consider the characteristics of different tasks, thus limiting the transferability.

To enable effective and transferable adversarial attacks, we first identify the fundamental obstacles. First, different VLP models are pre-trained with diverse architectures, learning objectives, and datasets, and are further fine-tuned for specific downstream tasks [1], [2], [3]. These variations lead different VLP models to rely on different features or patterns of images to make decisions, making it difficult to craft transferable adversarial perturbations. For instance, image-text retrieval returns relevant data from one modality for a query from the other by ranking the global image-text similarity between them, while image captioning generates descriptive text for an image by recognizing objects, understanding scenes, and capturing relationships. Thus, attacking retrieval models requires disrupting ranking orders based on global similarity, whereas attacking captioning models demands precise semantic manipulation to mislead content generation. Second, the heterogeneity between data adds another layer of complexity. Images and texts inherently differ in format and describe the same underlying content from distinct perspectives, each carrying diverse and complementary information. This causes the complex cross-modal interactions, making UAPs hardly maximally disrupt the learned cross-modal alignment. Finally, the data-independent nature of UAPs further makes it harder to achieve both effectiveness and transferability. Unlike sample-wise perturbations, UAPs are learned on the entire dataset, which cannot make use of specific characteristics and vulnerabilities of each sample. Since each sample follows its own patterns, UAPs have to be strong enough to break diverse patterns for effective attacks. As a result, the learning process often leads to shortcut exploitation, where UAPs overfit to specific model weaknesses, making them effective against source models (the attacking target during training) but ultimately causing overfitting and reducing transferability. In summary, understanding and manipulating complex cross-modal relationships in sample-, modality-, and task-agnostic settings is particularly challenging, hindering the development of effective and transferable attacks.

To overcome these obstacles, we propose Hierarchical Refinement Attack (HRA). HRA enhances the universal adversarial transferability by focusing on sample-level and optimization-level refinements to disrupt cross-modal alignments. First, HRA disentangles adversarial examples, treating original data and UAPs separately to better exploit cross-modal interactions. Specifically, a novel semantic-preserving data augmentation technique called ScMix is designed to increase data diversity and facilitate the exploration of cross-modal interactions. At the same time, we enhance both the global and local utilities of UAPs, which can avoid the generation of UAPs relying on shortcuts to surrogate models. Additionally, we investigate the optimization trajectory, which is closely related to overfitting. Overfitting often occurs when the optimization process of gradient-based methods converges to local optima. To mitigate this problem, we propose future-aware momentum, which incorporates historical gradients and predicted future gradients to regularize the current update and

prevent the optimization from local optima. Furthermore, we implement a simple yet effective adversarial text attack that leverages intra- and inter-sentence importance measures to extract influential words as uniform adversarial perturbations. Through extensive experiments, we demonstrate the effectiveness of the proposed method.

The main contributions of this work are summarized as follows:

- This paper identifies the key characteristics and challenges of universal attacks on VLP models, including the sample-agnostic, model-agnostic, and task-agnostic nature of UAPs, as well as the insufficient exploration of cross-modal interactions.
- A novel HRA method is proposed, which learn multi-modal universal adversarial perturbations. HRA performs hierarchical refinement of adversarial examples by disentangling adversarial data and making use of both past and future gradients to exploit intrinsic cross-modal interactions and regularize the optimization path, alleviating overfitting.
- Thorough experiments are conducted, including a wide range of target VLP models, downstream tasks and datasets, including cross-modal retrieval scenarios, visual grounding and other downstream tasks. The results demonstrate that the proposed method effectively improves the transferability of universal multimodal attacks.

Compared to our previous conference work, i.e., ETU [20], our HRA introduces several substantial improvements. First, we conduct a deeper and more comprehensive investigation into the challenges of achieving transferable universal attacks. Second, we design novel strategies to enhance transferability, i.e., future-aware Momentum. We compute both the previous and future gradients, which are closely related to overfitting. The future-aware momentum strategy effectively mitigates overfitting, resulting in more transferable attacks. Third, we expand our evaluation by comparing our method against a broader range of state-of-the-art approaches and testing it across more target and source models. We also provide more in-depth analysis to offer deeper insights into the task and further highlight the superiority of our proposed method.

The rest of the paper is organized as follows: Section II provides a brief review of related works. Section III presents a detailed introduction to our methodology. In Section IV, we conduct comprehensive experiments, including attacks on various VLP models, datasets, and downstream tasks, as well as ablation studies and visualizations, to demonstrate the effectiveness of the proposed method. Finally, Section V concludes the paper and discusses current limitations and potential directions for future research.

II. RELATED WORK

A. Vision-Language Pre-training

Digital and realistic worlds encompass diverse data types, e.g., image, text, audio, video, and so on. To better understand the world, vision-language models (VLMs) are designed to understand visual and language content, capture their relations and generate multimodal content. These models facilitate

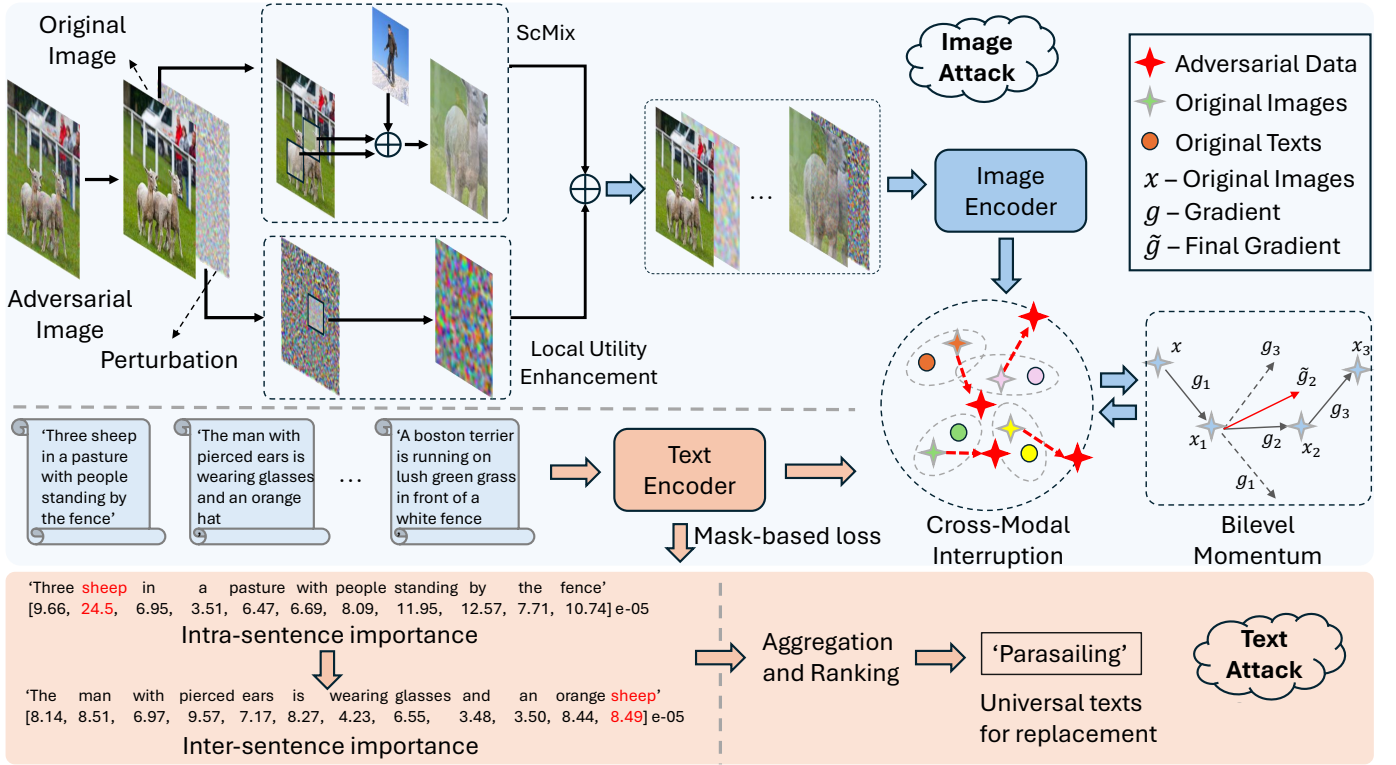


Fig. 1. An illustration of the proposed HRA framework, which hierarchically refines universal perturbations at both the sample level and the optimization level to improve transferability. Adversarial images consisting of the original images and adversarial perturbations are optimized in a disentangled manner to enlarge their discrepancy from the original paired data. The original images are augmented using ScMix, while the local utility of adversarial perturbations is enhanced. In addition, future-aware momentum leverages both historical and predicted future gradients to regularize the current gradient when refining universal image perturbations. Meanwhile, universal text perturbations are learned by intra- and inter-sentence importance measures and ranking.

diverse tasks e.g., image-text retrieval [22], [23], [24], image captioning [25], visual question answering [26], visual entailment [27], and so on [28], [1], [29]. VLMs typically require a large number of high-quality training data to establish effective prediction ability, which is time-consuming and restricted by the availability of large-scale data. To address these obstacles, vision-language pre-training (VLP) has been developed. It harnesses vast amounts of unlabeled multi-modal data, using self-supervised learning techniques to gain representative feature learning ability [30], [1], [2], [3]. VLP models exhibit outstanding generalizability and transferability, allowing adaptation to diverse datasets and downstream tasks through fine-tuning, thereby offering cost-effectiveness and flexibility. Representative VLP methods include CLIP [1], BLIP [30], ALBEF [2], and TCL [3]. CLIP aligns visual-linguistic modalities by projecting images and texts into a unified feature space, using contrastive learning to maximize similarity for matched pairs and increase the distance for unmatched pairs. BLIP [30] enhances dataset quality by synthesizing captions for web images, employing three contrastive learning objectives to jointly pre-train the model, i.e., image-text contrastive learning, image-text matching, and image-conditioned language modelling. ALBEF [2] first aligns unimodal representations of pair images and texts, and then fuses them with cross-modal attention to obtain joint representations. TCL [3] utilizes contrastive learning to perform both inter- and intra-modal alignment while preserving mutual information

between global and local representations in each modality.

B. Adversarial Attack

Real-world applications often involve uncertainty, randomness, and potential threats, making it crucial to ensure that developed models are both robust and secure. Adversarial attacks are one of the most effective methods for evaluating model robustness, which aims to induce incorrect predictions of target models by injecting imperceptible perturbations (i.e., adversarial perturbations) into input data [6], [14], [15], [7]. According to the scope, existing adversarial perturbations can be roughly categorized into sample-wise [8], [9], class-wise [31] and universal adversarial perturbations (UAPs) [32], [33], [34], which are designed for individual samples, specific classes, and all data, respectively. Generally, sample-wise and class-wise perturbations are more effective than universal perturbations as they can exploit vulnerabilities specific to each sample or class. However, they are less transferable to unseen data and must be generated from scratch for new samples or classes, limiting their scalability in large-scale applications. In contrast, universal perturbations are more efficient, as they can be reused across different data once learned. Nevertheless, since UAPs are independent of specific data, they fail to leverage data-specific characteristics and are more prone to overfit to target models during training, limiting their effectiveness and transferability.

1) *white-box and black-box attacks*: Early methods learn adversarial perturbations in *white-box* settings, assuming access to information about the victim models, tasks, and data [6], [14], [15]. However, in real-world applications, such target information might not be available and it is impractical to generate perturbations for all possible models, tasks, and datasets. Consequently, adversarial perturbations must often be learned in the *black-box* settings where target information is inaccessible, and the perturbations are required to be transferable to different models, tasks and data. However, due to factors like architectural differences, task variations and data distribution shifts, white-box attack methods would lose efficacy when applied to black-box scenarios. To address this challenge, current solutions primarily fall into two categories: *query-based attacks* [35], [36], [37] and *transfer-based attacks* [38], [39], [40]. Query-based attacks learn adversarial perturbations by analyzing models' feedback on perturbed inputs. As the inner architecture is not accessible, these attacks often estimate gradients using techniques like the finite difference approximation [36]. However, query-based attacks still require the existence of target models, limiting their practicality. Transfer-based methods overcome this limitation by leveraging substitute models, assuming that adversarial perturbations generated for one model may transfer to others. However, adversarial transferability is not always reliable due to differences in data representing caused by variations in model architectures and training schemes. Moreover, adversarial perturbations tend to overfit target models during training, reducing their effectiveness across different models. To improve adversarial transferability, various strategies have been proposed. For example, Lin *et al.* [41], [42] propose data augmentation to increase data diversity. Xiong *et al.* [43], [44] propose ensemble-based attacks, which train perturbations against multiple surrogate models, based on the intuition that perturbations effective against multiple models are more transferable. However, this approach requires access to multiple models and incurs additional computational costs. Dong *et al.* [10], [45], [46] develop momentum strategies to stabilize update directions and prevent perturbations from getting stuck in poor local optima by accumulating historical gradients. A more comprehensive discussion of these methods can be seen in the survey [7].

2) *Unimodal and multi-modal attacks*: Current methods primarily concentrate on unimodal cases, e.g., classification [6], [35], [45], where the objective is simply to disrupt the relationship between input data and its ground-truth label. In the real world, many scenarios involve multiple data modalities, e.g., image and text, leading to the development of multimodal models for tasks like image-text retrieval [22], [23], image captioning [25], and visual question answering [26]. To assess the robustness of multimodal models, multi-modal attack methods have been introduced, typically designed for specific tasks. For example, Zhang *et al.* [14], [15] learn adversarial perturbations to attack image-text searching models by maximizing the neighbourhood relationships defined by a similarity matrix. Yin *et al.* [16] produce adversarial perturbations to mislead visual question answering models by preventing a substitute large language model from giving correct answers for each

masked text. Since different tasks rely on distinct relationships between data modalities, attacks designed for one task often fail to transfer to others. This challenge has driven task-agnostic attack methods, including those for VLP models.

3) *Adversarial attack against VLP models*: To address this limitation, Zhou *et al.* [19] explore the use of universal adversarial patches, though their approach is restricted to CLIP. Additionally, the adversarial patch is not strictly constrained in perturbation magnitude, making it more susceptible to detection. To further improve universality and transferability, Zhang *et al.* [20] propose learning universal adversarial perturbations by enhancing their local utility and incorporating ScMix data augmentation to increase diversity and reduce overfitting.

Adversarial attacks against VLP models are still in their early stages, with only a few methods proposed. Compared to conventional multimodal attacks, attacking VLP models is more challenging due to the lack of access to downstream tasks and fine-tuning details. Existing methods primarily concentrate on the feature space and learn sample-wise perturbations by enlarging the feature distance between adversarial data and original data [17], [18], [12]. To further improve transferability, Lu *et al.* [18], [12] propose data augmentation to create more diverse image-text pairs, aiming to further exploit cross-modal interactions and mitigate overfitting. Despite the progress made, current approaches usually learn sample-wise perturbations, which are tailored to the specific characteristics and vulnerabilities of individual data samples. Consequently, when encountering new data, attackers have to learn tailored perturbations for each new data from scratch. This would incur huge computational costs and lead to less scalability for large-scale scenarios. To solve this, Zhou *et al.* [19] explore the use of universal adversarial perturbations, though their approach is restricted to CLIP. Zhang *et al.* [20] proposes to learn universal adversarial perturbations by enhancing their local utility and leveraging a ScMix data augmentation to promote data diversity to prevent overfitting. However, these methods focus solely on image-modality attacks and neglect the text modality, thereby limiting their effectiveness. Fang *et al.* [21] present an early attempt to generate both image and text attacks. Their method trains generators to produce adversarial examples by modeling data distributions, which risks overfitting to the source distribution. Moreover, it does not account for the characteristics of diverse downstream tasks and relies on an existing word library for text perturbation search, limiting its generality. In addition, the method generates adversarial text embeddings and then searches for semantically similar tokens in the corpus, creating a mismatch between embedding-level optimization and the final token-level perturbations.

III. PROPOSED METHOD

A. Preliminaries

The proposed HRA learns universal adversarial perturbations (UAPs) for both the image and text modalities in the black-box setting, where the target VLP models, datasets, and downstream tasks are unknown and inaccessible during training. To tackle this challenge, we introduce a transfer learning-based attack method that leverages a surrogate model

TABLE I

ATTACK SUCCESS RATE (%) ON IMAGE-TEXT RETRIEVAL. THE CLIP WITH THE ViT-B/16 AND FLICKR30K ARE ADOPTED AS THE SOURCE MODEL AND DATASET FOR TRAINING. THE GREY BACKGROUND INDICATES THE WHITE-BOX ATTACK RESULTS.

Target Model	Test Dataset	Flickr30K					
		Image-to-Text		Text-to-Image			
Task	Method	R@1	R@5	R@10	R@1	R@5	R@10
CLIP _{ViT-B/16}	HRA _L (image attack only)	88.96	76.43	70.43	93.49	88.27	85.32
	HRA _S (image attack only)	93.13	88.16	83.84	96.13	93.83	92.37
	HRA (image attack only)	88.47	78.61	73.07	92.69	87.5	84.89
Test Dataset		MSCOCO					
ALBEF	HRA _L (image attack only)	29.21	14.32	9.57	27.79	14.35	10.28
	HRA _S (image attack only)	24.65	12.20	8.60	25.58	12.92	9.22
	HRA (image attack only)	32.43	15.76	11.28	29.82	16.25	11.83

and dataset to generate UAPs capable of transferring across diverse models, datasets, and tasks.

Our approach is generic and does not impose specific assumptions about the surrogate model used during training. For example, some VLP models employ a multimodal encoder [2], [3], while others do not [1]. To ensure broad generality, we uniformly utilize the unimodal encoders available in each VLP model, i.e., the image encoder and the text encoder, denoted as f_I and f_T , respectively. Suppose a multi-modal dataset $\mathcal{D}_{src} = \{(x_i, y_i)\}_{i=1}^n$ is available for training, where (x_i, y_i) is an image-text pair and n is the number of pairs. The objective is to learn UAPs that can mislead other VLP models to incorrectly associate images and texts in a target dataset \mathcal{D}_{tar} at the reference time. For the image modality, we learn UAPs δ_I constrained by an l_∞ norm to ensure imperceptibility, i.e., $\|\delta_I\|_\infty \leq \epsilon_I$. Here, ϵ_I represents the perturbation magnitude. For the text modality, due to token discreteness, we implement a universal attack by consistently substituting a word in the text with a predefined replacement word. To maintain imperceptibility, the number of such substitutions is limited by a substitution budget ϵ_T .

1) *Vanilla Learning*: VLP models commonly bridge the gap between heterogeneous data, i.e., images and texts, by creating a shared representation space to associate images and texts with similar semantics. This makes it natural for an attacker to disturb the alignment between paired images and texts. Current methods usually only concentrate on the image modality. Specifically, given a surrogate model, UAPs for the image modality are learned by enlarging the feature distance between matched images and texts:

$$\arg \max_{\delta_I} \mathcal{L}_1(x, y, \delta_I) = \sum_{i=1}^n (\ell(f_I(x_i + \delta_I), f_I(x_i)) + \ell(f_I(x_i + \delta_I), f_T(y_i))), \quad (1)$$

where ℓ is a loss function to quantify the difference between representations of two samples, e.g., the KL-divergence loss.

Iterative methods such as PGD [47], [8] are usually used to solve the above objective. This scheme can effectively work in white-box scenarios, where data and models to attack during training are the same as those during testing. However, when applying learned UAPs to attack other different models, data, and tasks, i.e., black-box settings, UAPs would lose efficacy. We own this failure to several reasons. First, this vanilla UAP learning only enlarges the feature distance between surrogate image-text pairs on the source model, without considering the

generalization of UAPs to other models, tasks and datasets. Different VLP models have distinct architectures, training objectives and datasets across both pre-training and fine-tuning stages. These variations cause different models to rely on different features and patterns to associate modalities and make decisions. For example, image-text retrieval retrieves relevant data for a given query by ranking their similarity in the feature space, while Image captioning generates descriptive text for an image by recognizing objects, understanding scenes, and capturing relationships within the image. Attacking retrieval models requires disrupting ranking consistency, whereas misleading captioning models demands precise manipulation of semantic content. Second, vanilla UAP learning fails to account for the inherent heterogeneity between cross-modal data, limiting its ability to disrupt cross-modal alignment effectively. Since images and texts differ in format and provide diverse information, complex cross-modal interactions exist between them. As a result, simply increasing the feature distance between images and texts does not ensure maximal cross-modal misalignment. Lastly, UAPs are optimized over an entire dataset, requiring them to be robust against diverse sample patterns. To achieve this, the learning process often exploits shortcuts to the source model, generating perturbations that are highly specific to it. As a result, it leads to severe overfitting, reducing generalizability to unseen models and tasks. To enable effective and transferable attacks, it is crucial to improve cross-modal alignment disruption while reducing dependence on specific models, tasks, and data patterns.

B. Overview

To handle sample-, model- and task-independent challenges, we propose universal multimodal adversarial attacks with hierarchical refinement (HRA), which optimizes UAPs from two perspectives: cross-modal alignment and the optimization path. For the UAP learning of the image modality, HRA disentangles adversarial examples to separately deal with original data and UAPs. For original data, a novel ScMix data augmentation and benign adversarial perturbations are leveraged to increase data diversity, facilitating the exploration of cross-modal alignment and reducing reliance on specific data features and patterns. Additionally, both global and local regions of UAPs are reinforced to reduce dependence on specific global features and prevent the formation of shortcuts, thereby mitigating overfitting. Furthermore, HRA directly regularizes the optimization path, as overfitting occurs when the optimization drops into local optima. By incorporating both past and future gradients from vanilla learning, it stabilizes update directions, preventing convergence to local optima. For the text modality, the proposed method ranks word importance by masking individual tokens and measuring the divergence between the masked and original text representations, considering both intra-sentence and inter-sentence contexts. An illustration of the proposed HRA can be found in Fig. 1.

C. Disentangled Adversarial Images

1) *ScMix Augmentation*: Data augmentation is a well-established technique for improving adversarial transferability

by increasing data diversity [18]. In multi-modal attack scenarios, employing data augmentation can help further exploit cross-modal interactions.

Specifically, an effective data transformation for augmentation should meet two key criteria: diversity and semantic preservation. This means the augmentation should introduce visual differences between the original and augmented data while maintaining semantic integrity. If the transformation significantly alters semantics, the model may fail to recognize the data correctly, ultimately reducing the effectiveness of the generated image UAPs. Under this regime, we propose a novel semantic-preserving ScMix method. ScMix incorporates self-mix and cross-mix operations. In the self-mix process, new data is constructed by mixing different transformed versions of the same original image. Specifically, two subregions of an image x_i are randomly cropped and resized to match the original image size. Let x_i^1 and x_i^2 denote two rescaled subregions. They are then combined to create a new instance \hat{x}_i . Finally, the mixed instance is interpolated with another randomly selected image x_j from the mini-batch to generate the final augmented sample \tilde{x}_i . Formally, the whole process can be formulated as follows:

$$\begin{aligned} p_i &= \eta \cdot f_I(x_i^1) + (1 - \eta) \cdot f_I(x_i^2), \\ \tilde{x}_i &= \underbrace{\beta_1 \cdot \hat{x}_i + \beta_2 \cdot x_j}_{\text{Cross-mix}}, \\ \hat{x}_i &= \underbrace{\eta \cdot x_i^1 + (1 - \eta) \cdot x_i^2}_{\text{Self-mix}}, \end{aligned} \quad (2)$$

$$\text{s.t. } \eta = \max(\eta', 1 - \eta'), \eta' \sim \text{Beta}(\alpha, \alpha),$$

where $\beta_1 > \beta_2 \in [0, 1)$ ensures that the cross-mix does not significantly alter the original semantics when injecting another image. p represents the prediction for the ScMixed data. Beta(\cdot, \cdot) denotes a Beta distribution with $\alpha \in (0, \infty)$.

With ScMix, we can augment the original data to create diverse multi-modal data pairs. Furthermore, in datasets, e.g., Flickr30K [48] and MSCOCO [49], there often exists diverse captions that describe an image for different perspectives or language styles. We capture the most relevant captions for each image to further enhance multi-modal data diversity. Specifically, let the caption set for image x_i be $\{y_{i1}, y_{i2}, \dots, y_{ik}\}$. The augmented data pairs are $\{(\tilde{x}_{i1}, y_{i1}, p_{i1}), (\tilde{x}_{i2}, y_{i2}, p_{i2}), \dots, (\tilde{x}_{ik}, y_{ik}, p_{ik})\}$, where $\tilde{x}_{i1}, \tilde{x}_{i2}, \dots, \tilde{x}_{ik}$ are generated by applying ScMix to x_i . As a result, an enriched training set is obtained, which helps to better exploit cross-modal interactions and prevent overfitting.

Since UAPs are optimized across the entire dataset, applying data augmentation to increase data diversity for optimizing the full image UAPs may lead to overfitting. Table I presents some black-box attack results, where we observe that HRA_S that leverages the ScMix to optimize the entire UAP region, performs worse than HRA_L, which does not incorporate ScMix. To handle this, we propose leveraging ScMix to optimize local regions of image UAPs.

2) *Local Utility Enhancement*.: Enhancing the local utility of image UAPs alongside optimizing the entire perturbation can prevent UAPs from relying on specific features and

creating shortcuts to source models. Specifically, during the UAP learning process, we randomly crop subregions of UAPs and resize them to match the original image size. For brevity, we denote this transformation process as \mathcal{A}_s . Similar to optimizing the entire UAPs, the local regions of the UAPs are trained by enlarging the embedding distance between perturbed images and their original pairs:

$$\begin{aligned} \arg \max_{\delta_I} \mathcal{L}_2(x, y, \delta_I) &= \sum_{i=1}^{n_t} (\ell(f_I(x_i + \mathcal{A}_s(\delta_I)), f_I(x_i)) \\ &\quad + \ell(f_I(x_i + \mathcal{A}_s(\delta_I)), f_T(y_i)) \\ &\quad + \ell(f_I(\tilde{x}_i + \mathcal{A}_s(\delta_I)), f_I(x_i)) \\ &\quad + \ell(f_I(\tilde{x}_i + \mathcal{A}_s(\delta_I)), f_T(y_i)) \\ &\quad + \ell(f_I(\tilde{x}_i + \mathcal{A}_s(\delta_I)), p_i)), \end{aligned} \quad (3)$$

where n_t is the caption number.

The proposed local utility enhancement is effective for three key reasons. First, strengthening local regions naturally improves the overall effectiveness of image UAPs by making subregions more disruptive to various image patterns. This also facilitates disrupting cross-modal alignment across different samples, models and tasks, where diverse features are considered. Lastly, optimizing local regions acts as a form of model augmentation by introducing an extra transformation to image UAPs before feeding them into source models. This regularization effect helps mitigate overfitting, ensuring the perturbations remain effective across different scenarios.

3) *Overall objective*.: The overall objective for optimizing UAPs for images is defined as:

$$\arg \max_{\delta_I} \mathcal{L}(x, y, \delta_I) = \mathcal{L}_1(x, y, \delta_I) + \mathcal{L}_2(x, y, \delta_I), \quad (4)$$

where data in \mathcal{L}_1 and \mathcal{L}_2 would also be augmented with different captions for each image.

D. Future-Aware Momentum

HRA further refines image UAPs by directly regularizing the optimization path. Gradient-based methods optimize UAPs by calculating the gradient direction of the loss Eq. (4). However, in multi-round learning procedures, the update process would gradually converge to local optimal, causing overfitting [46], [40], [50], [41]. The momentum method is an effective approach for stabilising update directions by leveraging previous gradients and has been widely used in various robust learning methods [10], [45]. Classical momentum [46] typically relies on accumulated past gradients to regularize the optimization trajectory. However, since UAPs are optimized across the entire dataset, gradients based on historical perturbations may diverge from the current optimization direction. Moreover, such momentum only consider a limited optimization scope, i.e., the current and past, resulting in a narrow exploration space. To address this, we propose Hierarchical Momentum that considers both past gradient and future gradients to stabilize the optimization process and broaden the search scope, thereby further alleviating overfitting.

Algorithm 1: Hierarchical Refinement Attack

Require: Training data \mathcal{D} , mini-batch size l , iteration times M_I, M_T , parameters $\epsilon_I, \epsilon_T, \alpha, \beta_1, \beta_2, \gamma_1, \gamma_2, d$;

Require: Randomly initialize δ_I , initialize $g_p^0 = 0$;

// Image attack;

// Exploit diverse matching captions for each image to augment the dataset;

for $m_I = 1 \rightarrow M_I$ **do**

for $(x^{m_I}, y^{m_I}) \sim \mathcal{D}$ **do**

$(\tilde{x}^{m_I}, \tilde{y}^{m_I}) \leftarrow (x^{m_I}, y^{m_I})$ // Augment each image-text pair via ScMix according to Eq.(2);

$\mathcal{A}_s(\delta_I)$ // Randomly crop and resize UAPs;

$g^{m_I} \leftarrow \frac{1}{|x^{m_I}|} \nabla_{\delta_I^{m_I}} \mathcal{L}(x^{m_I}, y^{m_I}, \delta_I^{m_I})$ // Calculate the current gradient according to Eq.(5);

$g_f^{m_I} \leftarrow \frac{1}{|x^{m_I}|} \nabla_{\delta_I^{m_I}} \mathcal{L}_1(x^{m_I}, y^{m_I}, \delta_I^{m_I, d})$ // Calculate future gradients according to Eq.(7);

$\tilde{g}^{m_I} \leftarrow g^{m_I} + \gamma_1 \cdot g_p^{m_I-1} - \gamma_2 \cdot g_f^{m_I}$ // Update the gradient according to Eq.(8);

$\delta_I^{m_I} \leftarrow \text{Clip}_{\epsilon_I}(\delta_I^{m_I} + \alpha \cdot \text{sign}(\tilde{g}^{m_I}))$ // Update UAPs;

end

$g_p^{m_I} = \tilde{g}^{m_I}$ // Update the previous gradient;

end

// Text attack;

for $m_T = 1 \rightarrow M_T$ **do**

for $(x^{m_T}, y^{m_T}) \sim \mathcal{D}$ **do**

$S(w) = \ell(f_I(y^{m_T}), f_T(y^{m_T}))$ // Measure and record the importance of each word in a text sample according to Eq.(9);

end

end

$\delta_T \leftarrow \text{Rank}(S)$ // Rank the importance and select the important influential word as the perturbation;

return δ_I, δ_T ;

Specifically, denote the current mini-batch as (x^{m_I}, y^{m_I}) , where m_I is the training step. The gradient of the current optimization step is:

$$g^{m_I} \leftarrow \frac{1}{|x^{m_I}|} \nabla_{\delta_I^{m_I}} \mathcal{L}(x^{m_I}, y^{m_I}, \delta_I^{m_I}), \quad (5)$$

We also record the gradient of the last step:

$$g_p^{m_I-1} \leftarrow \frac{1}{|x^{m_I-1}|} \nabla_{\delta_I^{m_I-1}} \mathcal{L}(x^{m_I-1}, y^{m_I-1}, \delta_I^{m_I-1}), \quad (6)$$

The future gradient is calculated by:

$$g_f^{m_I} = \frac{1}{d} \sum_{i=1}^d g_f^d, \quad (7)$$

$$\text{s.t. } g_f^{m_I, d} \leftarrow \frac{1}{|x^{m_I}|} \nabla_{\delta_I} \mathcal{L}_1(x^{m_I}, y^{m_I}, \delta_I^{m_I+d}),$$

Where g_f denotes the mean gradient over the next d -step.

The previous gradient direction is less prone to overfitting, while the gradient direction from vanilla learning is more

susceptible to overfitting. Considering this, we regularize the current gradient using both the previous and future gradients as follows:

$$\tilde{g}^{m_I} \leftarrow g^{m_I} + \gamma_1 \cdot g_p^{m_I} + \gamma_2 \cdot g_f^{m_I, d}, \quad (8)$$

where $\gamma_1, \gamma_2 \in [0, 1]$ are balancing parameters.

E. Text Attack

Different from images, text is discrete in nature and highly sensitive to token replacements, which makes it impossible to directly learn universal text perturbations in the same way as image perturbations. To address this challenge, we propose a simple yet effective text attack based on word substitution using universal trigger words. Our universal text attack does not rely on any external resources. Instead, it identifies optimal substitution tokens directly from the training corpus.

To identify influential words for text attacks, the method first measures the importance of each token in every training sample (intra-sentence importance measures) and aggregates these scores over the entire dataset (inter-sentence importance measures). The importance of a word is computed by masking it in the input text and evaluating the semantic discrepancy between the masked representation and that of the original image-text pair:

$$S(w) = \ell(f_I(\hat{y}), f_T(y)) + \ell(f_I(\hat{y}), f_I(x)), \quad (9)$$

where w denotes a word. y and \hat{y} are the original text and its masked counterpart, respectively.

Specifically, the importance of each word in the original sample is first measured and the top- k most salient words in each sample are selected as candidates. Their global influence is then further assessed by randomly substituting one of these candidate words into other sentences and measuring the resulting semantic shift. Universal trigger words are finally obtained by ranking all candidate tokens according to their aggregated influence scores and choosing the highest-ranked ones. To preserve imperceptibility, we restrict the text perturbation budget to $\epsilon_T = 1$, allowing only one token substitution. At test time, we consider two attack variants: HRA_{ran} , which randomly replaces a word, and HRA_{imp} , which replaces the most important word as in [21].

F. Algorithm

The detailed algorithm is summarized in **Algorithm 1**. For the image attack, in each epoch, mini-batch data are randomly sampled from the dataset. Next, ScMix is leveraged to create diverse data pairs. Subsequently, the current gradient, previous gradient, and future gradient are computed to update the UAPs. The optimization process repeats until the maximum number of iterations is reached. For the text attack, the method computes the importance of each word and aggregates the scores across the entire dataset, from which the most influential words are selected to serve as universal perturbations.

TABLE II

THE ATTACK SUCCESS RATE (%) OF R@1 IN IMAGE-TEXT RETRIEVAL. GREY CELLS DENOTE WHITE-BOX ATTACK RESULTS. **BOLD** INDICATES THE BEST PERFORMANCE, AND * MARKS THE SECOND BEST.

Test Dataset			Flickr30K															
Target Model			CLIP															
Source Model	Method	I2T	ResNet50		ResNet101		ViT-B/16		ViT-B/32		ViT-L/14		ALBEF			TCL		
			I2T	T2I	I2T	T2I												
CLIP _{ViT-B/16}	AdvCLIP	19.12	27.58	15.33	17.29	76.07	76.58	15.83	24.29	11.58	17.85	3.96	7.83	18.02	20.67			
	SGA	38.44	48.23	33.84	38.35	92.39	93.78	20.49	32.22	17.79	24.03	8.45	12.51	10.01	15.41			
	ETU	56.83	61.27	52.49	54.27	88.47	92.69	22.58	33.70	20.86	28.54	13.14	17.28	18.55	21.57			
	FD-UAP	38.06	46.83	30.27	36.33	85.89	83.31	20.61	31.83	16.07	24.39	8.55	13.89	10.96	15.98			
	C-PGC	67.43	74.58	59.13	70.12	87.98	89.69	48.59	62.31	37.30	57.60	25.23	35.90	<u>43.84</u>	59.33			
	HRA _{ran}	<u>70.50</u>	84.46	<u>71.52</u>	<u>85.08</u>	86.75	94.14	45.15	<u>68.91</u>	<u>54.11</u>	79.77	<u>32.22</u>	<u>57.65</u>	43.52	<u>62.57</u>			
	HRA _{imp}	76.63	88.54	77.39	88.99	90.55	95.72	54.97	79.35	61.84	85.73	40.98	70.28	52.37	76.95			
CLIP _{ResNet50}	AdvCLIP	78.77	82.64	22.99	27.72	6.01	13.85	15.21	24.36	10.06	15.59	3.55	7.46	17.61	20.69			
	SGA	98.16	98.68	27.71	36.43	10.92	16.33	17.55	25.45	10.31	19.07	5.74	9.92	6.85	12.67			
	ETU	95.79	<u>98.63</u>	37.04	44.94	9.33	17.49	16.58	27.74	9.82	18.65	5.42	10.59	18.55	21.57			
	FD-UAP	78.80	89.81	12.90	19.45	6.01	12.27	14.85	23.36	7.61	15.69	4.90	8.35	6.11	11.33			
	C-PGC	92.34	91.77	<u>68.45</u>	76.47	<u>31.17</u>	<u>48.87</u>	<u>40.25</u>	<u>59.18</u>	<u>30.06</u>	48.36	17.52	34.14	<u>22.76</u>	<u>42.38</u>			
	HRA _{ran}	94.76	96.57	63.60	<u>77.29</u>	29.20	48.61	32.15	51.80	25.15	<u>51.97</u>	<u>19.19</u>	<u>36.13</u>	21.29	36.88			
	HRA _{imp}	95.27	97.26	79.82	87.24	37.67	62.24	42.33	65.59	33.25	67.11	30.03	53.95	34.14	54.76			
ALBEF	AdvCLIP	19.41	27.62	13.67	17.22	8.96	15.34	17.18	25.35	9.94	17.46	63.19	63.38	37.72	36.76			
	SGA	18.14	25.28	11.37	17.26	6.99	12.79	16.69	23.71	8.10	15.59	74.87	72.99	18.65	19.62			
	ETU	26.56	35.03	20.31	25.08	10.06	17.72	17.18	26.22	13.01	21.55	83.00	87.07	32.98	31.50			
	FD-UAP	20.43	30.19	12.90	19.01	8.83	14.66	17.55	25.29	9.94	17.91	67.47	63.49	27.82	25.69			
	C-PGC	44.32	55.92	<u>36.02</u>	50.94	29.69	42.14	<u>39.75</u>	<u>53.99</u>	30.55	45.46	84.36	81.10	43.94	50.57			
	HRA _{ran}	<u>53.26</u>	66.93	<u>36.02</u>	<u>53.00</u>	<u>30.92</u>	48.97	33.87	46.07	32.64	49.71	<u>88.01</u>	<u>88.38</u>	<u>55.85</u>	<u>56.71</u>			
	HRA _{imp}	60.28	75.71	52.87	69.98	40.98	60.02	46.26	59.57	41.10	60.89	91.76	92.42	65.12	69.24			
TCL	AdvCLIP	24.27	35.68	17.62	22.74	8.22	16.33	17.18	28.16	11.41	19.78	23.15	24.58	60.17	54.12			
	SGA	20.31	29.16	13.28	19.38	7.36	13.66	16.97	25.19	9.45	18.65	18.87	20.65	83.63	86.37			
	ETU	27.59	39.69	20.82	26.96	9.20	17.94	17.44	28.61	12.64	20.59	23.25	25.44	<u>94.10</u>	87.60			
	FD-UAP	18.14	27.92	10.98	17.22	7.85	14.50	16.07	25.26	9.20	17.69	13.56	18.26	67.47	63.49			
	C-PGC	48.15	60.03	38.19	53.93	32.68	45.65	<u>38.90</u>	51.90	<u>34.48</u>	49.55	37.02	42.26	85.88	76.10			
	HRA _{ran}	<u>52.36</u>	72.42	52.23	70.67	32.76	65.59	36.20	62.27	32.27	63.79	53.28	63.24	91.15	90.98			
	HRA _{imp}	63.22	79.93	58.24	81.30	41.84	76.97	47.36	73.90	42.58	76.03	64.13	77.03	94.20	94.38			
Test Dataset			MSCOCO															
CLIP _{ViT-B/16}	AdvCLIP	35.78	44.71	25.07	11.38	82.18	81.77	31.63	38.89	38.23	38.72	13.56	16.04	29.15	30.24			
	SGA	96.49	<u>95.62</u>	<u>56.03</u>	59.45	96.49	95.62	41.55	46.68	36.44	41.41	23.25	23.45	24.74	24.15			
	ETU	78.55	79.37	72.01	73.59	93.55	94.25	45.14	50.51	43.49	47.35	32.43	29.82	34.02	30.28			
	FD-UAP	64.61	66.89	54.53	56.51	88.55	86.40	42.88	48.34	38.99	40.17	24.57	24.66	25.90	24.84			
	C-PGC	87.29	89.36	82.71	86.80	95.76	74.40	<u>80.89</u>	69.13	77.25	<u>54.68</u>	55.39	<u>72.41</u>	<u>76.33</u>				
	HRA _{ran}	<u>87.37</u>	<u>91.84</u>	<u>86.11</u>	<u>91.74</u>	96.38	97.01	<u>65.01</u>	80.05	78.02	<u>88.06</u>	53.49	<u>68.76</u>	58.92	72.54			
CLIP _{ResNet50}	AdvCLIP	93.87	95.07	42.46	45.53	16.12	23.44	26.82	37.27	23.04	27.41	15.26	16.36	29.60	29.52			
	SGA	97.06	97.83	50.02	55.55	23.92	29.28	31.90	39.02	29.91	33.66	16.68	18.64	18.61	21.05			
	ETU	96.64	97.3	61.26	64.95	25.79	31.70	31.63	40.27	30.52	33.09	17.99	20.00	20.97	23.10			
	FD-UAP	83.12	89.63	26.40	32.17	17.09	22.68	28.46	36.74	21.52	27.47	13.20	16.43	15.82	19.68			
	C-PGC	95.79	96.99	<u>87.13</u>	90.12	<u>62.80</u>	<u>72.42</u>	<u>65.62</u>	<u>77.77</u>	<u>57.65</u>	<u>67.67</u>	<u>42.36</u>	<u>54.75</u>	<u>47.78</u>	<u>59.18</u>			
	HRA _{ran}	97.38	<u>98.11</u>	82.96	88.28	48.72	62.85	<u>51.35</u>	<u>65.31</u>	48.95	64.21	41.35	51.95	41.59	51.53			
	HRA _{imp}	98.77	98.74	91.79	95.22	72.64	81.72	69.17	81.64	70.74	80.86	71.16	78.77	94.15	94.50			
ALBEF	AdvCLIP	39.76	45.36	27.09	32.51	22.28	26.42	32.20	39.77	25.83	30.04	68.68	64.60	56.27	50.19			
	SGA	36.90	41.82	23.54	30.94	18.58	24.37	30.87	38.20	22.36	28.20	85.51	82.43	32.54	27.62			
	ETU	49.90	56.11	40.42	45.16	25.6	31.95	33.57	41.47	34.38	37.32	82.99	85.19	50.90	42.04			
	FD-UAP	39.64	45.24	28.16	34.59	19.57	26.15	31.13	39.24	26.71	31.48	69.32	68.74	39.02	33.55			
	C-PGC	68.78	74.95	64.20	71.83	<u>57.19</u>	<u>65.07</u>	<u>62.95</u>	<u>71.76</u>	58.49	66.09	<u>91.88</u>	87.19	<u>77.33</u>	71.94			
	HRA _{ran}	<u>73.60</u>	<u>80.76</u>	68.61	67.46	55.74	64.91	56.96	69.03	60.47	67.26	90.85	91.02	70.34	65.71			
	HRA _{imp}	82.26	88.29	78.38	84.67	69.52	77.54	70.74	80.86	71.16	72.59	78.99	88.09	83.20	84.63			
TCL	AdvCLIP	47.32	54.57	36.04	42.29	24.80	29.74	33.31	41.69	29.11	32.26	45.13	37.25	93.89	89.00			
	SGA	37.39	45.86	28.36	33.89	21.14	25.57	31.13	39.46	26.44	30.97	30.69	40.86	92.28	88.57			
	ETU	53.25	57.99	42.30	46.58	26.40	31.90	33.88	41.78	31.48	33.83	45.42	37.93	93.28	89.45			
	FD-UAP	38.58	44.07	25.58	31.58	20.49	26.06	29.65	38.01	27.24	30.42	31.92	28.46	83.97	78.65			
	C-PGC	72.70	79.97	66.20	75.18	<u>63.49</u>	68.28	<u>64.33</u>	72.08	<u>64.36</u>	70.09	64.78	61.66	93.57	87.43			
	HRA _{ran}	<u>78.59</u>	<u>87.96</u>	<u>73.89</u>	<u>84.74</u>	60.47	<u>83.25</u>	58.18	<u>78.27</u>	58.60	<u>82.43</u>	<u>74.32</u>	<u>73.10</u>	<u>94.21</u>	<u>93.72</u>			
	HRA _{imp}	86.80	94.17	83.16	93.43	72.80	93.23	71.42	90.63	71.16	92.59	78.99	88.09	96.32	96.22			

IV. EXPERIMENTS

A. Settings

Downstream tasks and datasets. To comprehensively evaluate the performance of the proposed method, we conduct experiments on four vision-language tasks with three datasets.

Tasks include the image-text retrieval, the image captioning, and the visual grounding. The image-text retrieval aims to find relevant data from a modality based on a query from another modality. This task consider the ranking between different modalities. Image captioning endeavours to generate a descriptive textual caption for a given image, which requires a model to capture details of visual data. Visual grounding is to

associate textual descriptions with specific regions or objects in an image, which requires

including vision transformers (i.e., ViT-B/16, ViT-B/32, and ViT-L/14[52]) and CNNs (i.e., ResNet50, and ResNet101 [53]). The text encoder is a 6-layer transformer. For BLIP, we choose the one that consists of a ViT-B/16 and a 6-layer transformer as the image and text encoder to attack. In addition, BLIP is mainly used for experiments on the image captioning task. ALBEF and TCL take ViT-B/16 as the image encoder and adopt a 6-layer transformer for both the text encoder and multimodal encoder.

Evaluation metric. For image-text retrieval, we utilize the Attack Success Rate (ASR) as a metric to quantify the effectiveness of the proposed attack and all compared baselines. ASR is calculated as the percentage of adversarial examples that successfully deceive the model, providing a reliable measure of the attackers' effectiveness. For other tasks, we compare the performance of VLP models on adversarial examples with their performance on the original examples.

Implementation details. For the fundamental experiments, we set the perturbation magnitudes to $\epsilon_I = 12/255$ for images and $\epsilon_T = 1$ for texts. We further evaluate the proposed method under varying perturbation budgets. PGD is utilized to solve the optimization problem for the image attack, with the number of iterations $M_I = 100$ and the step size as $\alpha = \epsilon_I/M_I * 1.25$. The batch size is set as 16. $\beta_1 = 0.8$, $\beta_2 = 0.2$, $\gamma_1 = 0.9$, $\gamma_2 = 0.1$, $M_T = 15$. For ℓ , we employ the KL-divergence to quantify the discrepancy between two samples.

Baselines. We compare our approach with several state-of-the-art methods, including:

- AdvCLIP [19], which generates UAPs by breaking neighbourhood relationships between images and texts;
- SGA [34], which divides large-batch learning into several small-batch learning and aggregates gradients of small-batch data to enhance the gradient stability and avoid dropping into local optima;
- ETU [20], which utilizes ScMix augmentation to increase input diversity and enhances the local utility of UAPs;
- FD-UAP [54], which is proposed to destroy significant features while strengthening the less significant features at low-level layers;
- C-PGC [21] uses conditional generators to learn adversarial image and text embeddings by enlarging their discrepancy from the original data while aligning them with the farthest samples. Text perturbations are obtained by searching for words in a corpus that are semantically similar to the learned adversarial text embeddings.

AdvCLIP, SGA, ETU, and FD-UAP focus solely on image-modality attacks, whereas C-PGC and the proposed HRA support attacks on both the image and text modalities.

Evaluation Preparation. We assess the transferability of the proposed method by launching attacks against a range of VLP models, i.e., CLIP models with different backbones, ALBEF and TCL, in black-box settings. Given that different VLP models may accept inputs of varying sizes, the learned UAPs are resized accordingly before initiating attacks. For instance, UAPs learned on CLIP are resized from 224×224 to 384×384 for attacks on ALBEF/TCL, whereas UAPs from ALBEF/TCL to CLIP are resized to 224×224 .

B. Cross-model Transferability

Table II summarizes the attack performance on both image-to-text and text-to-image retrieval tasks, using various source models and the Flickr30K dataset for training. From these results, we draw the following observations.

1) *Comparison with baselines:* All methods exhibit substantial performance degradation when transferred to unseen models and datasets, confirming that different models rely on distinct feature representations and thus present a significant model gap. Notably, UAPs remain highly effective on the same model even when evaluated on different datasets. For example, UAPs generated on CLIP_{ViT-B/16} transfer well from Flickr30K to MSCOCO. This indicates that existing attacks tend to produce perturbations that are strongly model-specific.

The inferiority of compared methods largely comes from insufficient consideration of characteristics of UAPs, including model- and data-agnostic natures, as well as cross-modal interactions. From the perspective of the image modality, AdvCLIP generates UAPs by destroying neighbourhood relationships in the source models, but fails to account for this in the target model. FD-UAP focuses on capturing model-agnostic cues from low-level features, but fails to exploit cross-modal interactions, limiting its transferability. In contrast, our disentangled adversarial example refinement strategy, i.e., incorporating ScMix augmentation and local utility enhancement, effectively explores cross-modal alignment and captures the data-independent nature of UAPs. It enables more reliable disruption of cross-modal relationships across models (as demonstrated by the results of our conference version, ETU, and the proposed HRA).

In addition, C-PGC produces both image and textual UAPs conditioned on the training distribution. This makes it rely on model-dependent features, limiting its ability to transfer to unseen models. SGA attempts to alleviate overfitting by aggregating gradients from other mini-batches. However, aggregating gradients from many mini-batches may dilute the relevance of the update direction, which explains its limited improvements, particularly on CLIP_{ViT-L/14} and ALBEF in Table II. In comparison, our method utilizes both previous and estimated future gradients to regularize the current gradient, providing more informative update guidance and achieving superior transferability.

2) *Effects of multimodal attacks:* Incorporating text attacks further enhances the attack performance, as evidenced by clear gains of C-PGC and HRA over other methods. Replacing the most salient words yields additional improvements, which is reflected in the superior performance of HRA_{imp} compared with HRA_{ran}. Interestingly, although C-PGC also replaces the most important words, our HRA_{ran} still performs better in many cases, indicating the effectiveness of directly discovering substitution words rather than learning universal embeddings and then mapping them back to tokens. Moreover, our method does not rely on a predefined word library, further demonstrating its practicality. It is also noted that identifying the most important words would incur additional computational overhead (i.e., HRA_{imp}), while our HRA_{ran} avoids.

TABLE III

ATTACK PERFORMANCE ON IMAGE CAPTIONING. THE TRAINING DATASET AND TEST DATASET ARE FLICKR30K AND MSCOCO, RESPECTIVELY. BLIP IS TAKEN AS THE TARGET MODEL. “BASELINE” DENOTES THE PERFORMANCE OF THE TARGET MODEL ON ORIGINAL DATA. LOWER VALUES REPRESENT BETTER ADVERSARIAL TRANSFERABILITY. **BOLD** INDICATES THE BEST PERFORMANCE, AND * MARKS THE SECOND BEST.

Source Model	CLIP _{ViT-B/16}					ALBEF				
	B@4	METEOR	ROUGE_L	CIDEr	SPICE	B@4	METEOR	ROUGE_L	CIDEr	SPICE
Baseline	39.31	30.69	59.62	131.38	23.52	39.31	30.69	59.62	131.38	23.52
AdvCLIP	38.20	30.03	58.70	127.14	22.88	36.59	29.15	57.35	121.79	21.95
SGA	36.10	28.89	57.25	120.47	21.85	33.92	27.67	55.41	112.28	20.62
ETU	<u>34.83</u>	<u>28.07</u>	<u>56.29</u>	<u>114.81</u>	<u>21.02</u>	<u>33.42</u>	<u>27.28</u>	<u>54.96</u>	<u>109.34</u>	20.11
FD-UAP	35.91	28.78	57.15	119.63	21.65	34.37	28.09	56.02	113.26	20.86
C-PGC	35.63	28.44	56.75	117.33	21.38	33.97	27.73	55.50	112.69	20.50
HRA	32.41	26.80	54.31	106.60	19.61	<u>32.67</u>	<u>27.21</u>	<u>54.62</u>	108.19	<u>20.15</u>

TABLE IV

ATTACK PERFORMANCE ON VISUAL GROUNDING. THE TRAINING AND TEST DATASET ARE FLICKR30K AND REFcocO+, RESPECTIVELY. ALBEF BUILT FOR VISUAL GROUNDING IS USED AS THE TARGET MODEL. THE “BASELINE” DENOTES THE PERFORMANCE OF THE TARGET MODEL ON THE ORIGINAL DATA. LOWER VALUES REPRESENT BETTER ADVERSARIAL TRANSFERABILITY. **BOLD** INDICATES THE BEST PERFORMANCE, AND * MARKS THE SECOND BEST.

Source Model	CLIP _{ViT-B/16}			ALBEF		
	Val	TestA	TestB	Val	TestA	TestB
Baseline	51.24	56.71	44.79	51.24	56.71	44.79
AdvCLIP	<u>50.45</u>	<u>54.49</u>	<u>43.32</u>	48.21	<u>52.48</u>	40.99
SGA	49.43	53.95	42.46	<u>47.64</u>	52.79	38.58
ETU	48.50	51.54	41.66	<u>45.49</u>	49.70	38.00
FD-UAP	49.09	52.74	42.28	46.08	51.36	36.53
C-PGC	41.59	44.22	36.74	39.22	42.82	33.83
HRA _{ran}	<u>34.21</u>	<u>34.93</u>	<u>31.85</u>	<u>32.60</u>	<u>32.80</u>	28.00
HRA _{imp}	32.85	33.86	31.74	31.58	32.01	28.37

3) *Effects of learning objectives*: Learning objectives also influence transferability. Models trained with similar objectives tend to exhibit stronger adversarial transferability, as observed in attacks across different CLIP variants and other architectures. For instance, UAPs generated on one CLIP model transfer better to other CLIP models than to ALBEF or TCL.

4) *Asymmetry of attacks*: Interestingly, adversarial transferability is asymmetric. strong transfer in one direction does not necessarily imply strong transfer in the opposite direction, e.g., from CLIP_{ViT-B/16} to CLIP_{ResNet50}. This asymmetry may arise because certain models can capture features learned by others, while the reverse is not true.

These results and analyses demonstrate that adversarial transferability is shaped by multiple factors, including data properties, model architectures, learning objectives, and cross-modal interactions. This highlights the importance of accounting for these factors when designing transferable attacks.

C. Cross-task Transferability

We evaluate the effectiveness of the proposed method across different tasks, including image–text retrieval, visual grounding, and image captioning.

1) *From image-text retrieval to other tasks*: We first examine transfer attacks from image–text retrieval to visual grounding and image captioning, with results presented in Tables IV and III, respectively. For both experiments, we generate

UAPs using CLIP_{ViT-B/16} and ALBEF as the source models and Flickr30K as the source dataset. For visual grounding, we use ALBEF and RefCOCO+ as the target model and dataset. For image captioning, we use BLIP and MSCOCO as the target model and dataset.

Across both tasks, all methods exhibit notably reduced transferability. This is expected due to substantial differences in data distributions, model architectures, and task objectives. Different tasks encourage models to learn distinct feature representations and thus possess different vulnerabilities. For instance, image–text retrieval focuses on global cross-modal similarity, whereas image captioning requires fine-grained visual understanding and linguistic generation. Consequently, UAPs that degrade retrieval features may not effectively disrupt captioning models.

Nevertheless, the proposed method achieves the strongest universal adversarial performance. This is attributed that it captures both local and global utilities of UAPs and increases data diversity to explore cross-modal interactions at multiple granularities. The future-aware momentum further alleviates overfitting, and the incorporation of text attacks adds complementary cross-modal disruption.

2) *From visual grounding to image-text retrieval*: We also evaluate transfer attacks from visual grounding to image–text retrieval, with results provided in Table V. The consistent improvements across models further demonstrate the effectiveness of the proposed method.

In summary, the strong performance on both cross-model and cross-task transfer scenarios verifies the effectiveness and generality of the proposed approach.

D. Parameter analysis

1) *Influence of Perturbation Budgets*: The perturbation magnitude plays a crucial role in balancing attack effectiveness and imperceptibility. A small budget may fail to generate sufficiently disruptive perturbations, whereas a large budget can degrade visual quality and make the attack more easily detectable. Figure 2 and 3 summarize the results under varying perturbation magnitudes for image and text attacks respectively, which demonstrate our statement. Specifically, as the magnitude of UAPs increases, the performance of attacks increases. In addition, across all magnitudes, the proposed method consistently achieves the best performance, further verifying its superiority.

TABLE V

THE ATTACK SUCCESS RATE (%) OF R@1 UNDER TRANSFER ATTACK FROM VISUAL GROUNDING ON REFCOCO+ TO IMAGE-TEXT RETRIEVAL ON FLICKR30K AND MSCOCO. **BOLD** INDICATES THE BEST PERFORMANCE, AND * MARKS THE SECOND BEST.

Test Dataset			Flickr30K													
Target Model		CLIP														
Source Model	Method	ResNet50		ResNet101		ViT-B/16		ViT-B/32		ViT-L/14		ALBEF		TCL		
		I2T	T2I													
ALBEF																
ALBEF	AdvCLIP	11.88	19.52	0.26	0.38	0.12	0.48	13.13	20.36	8.10	15.01	2.29	4.58	4.03	7.31	
	SGA	16.86	26.48	13.03	17.56	6.26	11.98	30.83	41.35	7.98	16.27	8.09	11.74	3.27	6.71	
	ETU	20.31	28.68	14.56	19.55	10.80	16.49	19.02	28.12	11.41	18.91	15.95	28.74	11.49	15.00	
	FD-UAP	18.26	28.27	11.75	17.29	6.13	12.31	16.93	23.97	8.34	15.82	30.39	49.60	10.12	14.21	
	C-PGC	35.55	51.89	31.14	47.74	21.31	31.00	22.07	49.44	18.42	34.10	28.47	53.11	27.61	40.83	
	HRA _{ran}	36.40	48.44	31.16	44.94	22.33	33.15	26.01	41.66	20.12	36.28	37.64	55.52	31.09	42.71	
	HRA _{imp}	45.98	62.92	40.49	59.83	28.83	46.81	35.83	55.12	30.67	50.55	46.51	66.46	41.31	57.71	
Test Dataset																
MSCOCO																
ALBEF	AdvCLIP	23.13	34.36	0.41	0.95	0.19	0.76	24.30	32.06	18.50	24.89	7.04	10.92	8.02	11.83	
	SGA	34.57	42.08	25.87	32.28	19.08	23.85	14.97	26.06	22.97	28.21	16.94	22.23	12.14	13.02	
	ETU	39.76	47.38	32.04	38.04	27.70	32.41	35.75	43.31	30.68	33.85	34.49	49.26	27.57	24.64	
	FD-UAP	36.62	42.38	22.68	30.79	17.36	21.38	30.10	37.39	21.06	26.61	41.49	48.88	22.80	21.88	
	C-PGC	43.55	61.89	36.14	57.74	30.31	51.00	36.07	59.44	24.42	49.10	35.94	53.40	28.49	38.47	
	HRA _{ran}	60.24	69.33	51.53	65.46	43.95	55.47	44.49	59.87	44.03	56.40	37.64	55.52	31.09	42.71	
	HRA _{imp}	73.93	81.58	66.29	79.25	60.05	71.66	62.34	74.97	61.58	71.30	46.51	66.46	41.31	57.71	

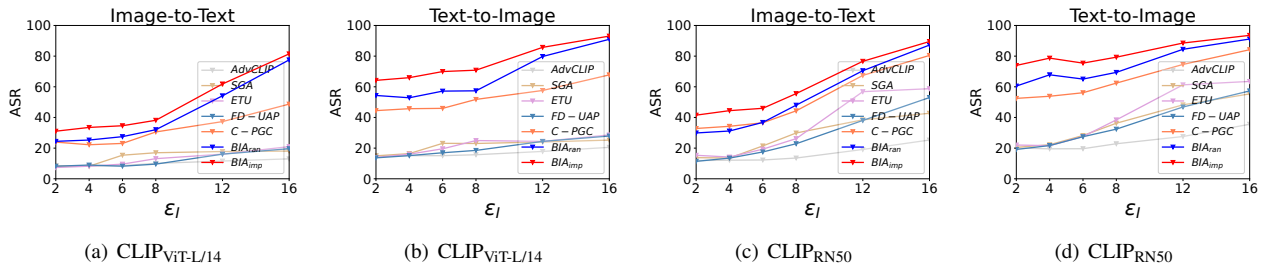


Fig. 2. The attack success rate in terms of the average of R@1 in image-text retrieval on Flickr30K under different magnitudes of the image UAPs. The source model is ViT-B/16-based CLIP.

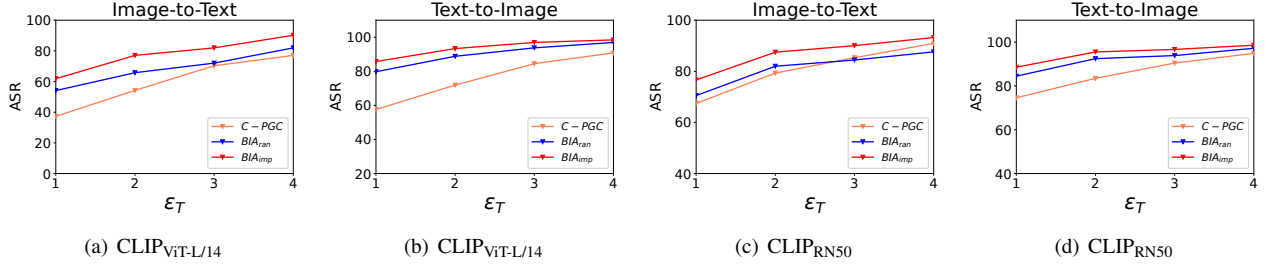


Fig. 3. The attack success rate in terms of the average of R@1 in image-text retrieval on Flickr30K under different magnitudes of the text UAPs. The source model is ViT-B/16-based CLIP.

2) *Influence of Combination Weights in Future-Aware Momentum:* We further analyze the role of past and future gradients by evaluating attack performance under different weighting schemes. We take HRA_{imp} as an example, and the corresponding results are shown in Figure 4. From the figures, we can have the following observations. For past gradients, very small weights are insufficient to meaningfully regularize the current update, whereas excessively large weights overly constrain the optimization to previous directions and weaken the attack. For future gradients, small weights already provide beneficial guidance by anticipating upcoming trends, while large weights lead to overfitting.

3) *Influence of the Number of Future Steps:* To investigate how future gradients contribute to improved transferability, we use HRA_{imp} as an example and report the attack performance

in Figure 5. The results show that a longer update horizon generally enhances performance. However, in some cases, an excessively long horizon begins to degrade it. For example, when attacking CLIP_{ViT-L/14}, extending the horizon from 1 to 2 steps improves transferability, whereas further increasing it from 2 to 4 steps leads to a slight performance drop. This degradation occurs because too many update steps cause the perturbation to overfit the source model's gradients, thereby weakening its transferability to other models.

In terms of computational cost, on a workstation equipped with an NVIDIA L40s GPU, the training time of the proposed method with a number of steps of 0, 1, 2, 3, 4 is 229, 309, 553, 675, 675, respectively. Overall, step = 2 provides the best trade-off between performance and efficiency,

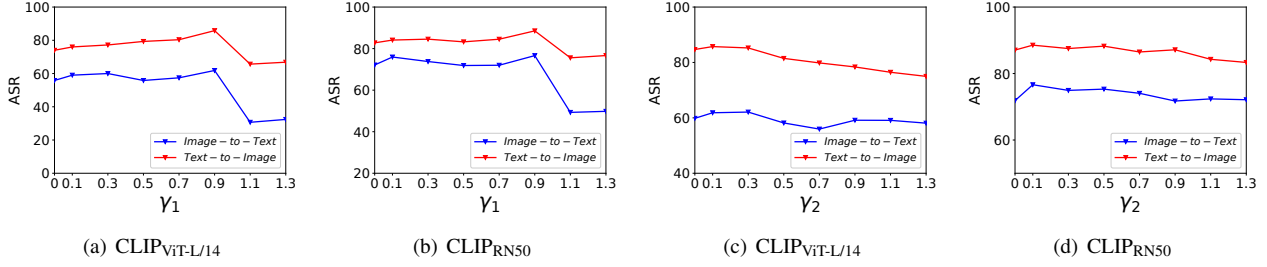


Fig. 4. The attack success rate in terms of the average of R@1 in image-text retrieval on Flickr30K under different weights of the past and future gradients. The source model is ViT-B/16-based CLIP.

TABLE VI

ABLATION STUDY OF DIFFERENT COMPONENTS ON FLICKR30K. THE ATTACK SUCCESS RATE OF R@1 ON IMAGE-TEXT RETRIEVAL IS REPORTED. CLIP_{ViT-B/16} IS ADOPTED AS THE SOURCE MODEL.

Target Model	CLIP										ALBEF		TCL	
	RN50		RN101		ViT-B/16		ViT-B/32		ViT-L/14		I2T		T2I	
Method	I2T	T2I	I2T	T2I	I2T	T2I	I2T	T2I	I2T	T2I	I2T	T2I	I2T	T2I
HRA _{imp} w MixUp	71.73	86.64	74.97	88.22	90.67	96.81	54.85	79.25	61.29	83.79	40.46	69.43	51.90	75.36
HRA _{imp} w BSA	66.75	80.88	69.99	85.21	94.60	94.46	50.34	77.73	55.71	75.10	40.25	68.92	51.32	73.88
HRA _{imp} w TIA	68.50	82.32	69.09	85.76	94.11	88.72	51.46	76.25	54.36	74.74	38.27	68.43	52.05	73.86
HRA _{imp} w SIA	64.09	82.39	68.84	85.63	74.72	95.04	52.02	77.44	49.57	75.32	37.64	68.36	50.47	75.52
HRA _{imp} w Mom	71.86	87.06	70.85	82.27	35.71	69.68	52.58	77.48	59.83	85.48	36.13	68.44	49.30	74.93
HRA _{imp} w/o BM	67.69	79.62	66.67	80.51	91.41	94.59	41.35	67.78	39.26	60.82	34.10	68.50	48.79	75.98
HRA _{imp} w/o ScMix	72.54	84.70	72.03	85.73	95.34	96.91	50.06	78.51	47.36	72.42	33.30	66.10	49.53	76.67
HRA _{imp} w/o LUE	72.80	83.22	69.73	84.97	94.72	96.13	52.88	79.16	43.68	73.42	33.99	68.15	47.42	74.76
HRA _{imp} w/o ScMix&LUE	72.03	81.17	69.22	80.31	95.58	97.00	48.02	77.84	40.98	70.14	30.10	64.50	46.79	72.98
HRA _{imp} w/o ScMix&BM	72.29	83.22	69.99	84.91	95.09	95.36	48.90	76.32	38.42	67.65	29.83	61.55	45.37	69.29
HRA _{imp} w/o LUE&BM	63.22	82.33	59.51	82.90	87.12	88.72	48.96	78.77	40.25	71.88	32.33	65.43	46.05	76.07
HRA _{imp} w/o ScMix&LUE&BM	62.84	74.55	58.49	75.71	94.23	96.84	42.09	68.56	40.47	63.92	30.06	63.83	42.68	73.48
HRA _{imp} w/o Text attack	67.43	76.35	65.52	74.52	80.49	89.34	28.34	45.72	36.81	66.33	20.33	21.23	24.34	24.38
HRA _{imp} w/o Image attack	40.49	74.37	41.63	74.65	36.32	67.88	41.47	64.84	32.02	61.56	22.73	57.95	35.30	69.12
HRA _{imp}	76.63	88.54	77.39	88.39	99.05	95.27	54.97	79.35	61.84	85.73	40.98	70.28	52.37	76.95

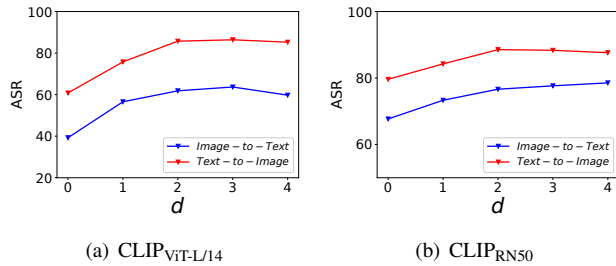


Fig. 5. The attack success rate in terms of the average of R@1 in image-text retrieval on Flickr30K under different numbers of future gradient steps. The source model is ViT-B/16-based CLIP.

and the associated computational overhead remains acceptable.

E. Ablation study

To verify the effectiveness of the proposed method, we conduct extensive ablation studies using HRA_{imp} as an example. First, we evaluate the contribution of each component by removing them individually, resulting in HRA_{imp} w/o LUE (local utility enhancement), HRA_{imp} w/o ScMix, and HRA_{imp} w/o FM (future-aware momentum). We also examine combinations of component removals, including HRA_{imp} w/o LUE&ScMix, HRA_{imp} w/o LUE&FM, HRA_{imp} w/o ScMix&FM, and HRA_{imp} w/o ScMix&LUE&FM. Second, we assess the roles of image and text attacks by disabling

each separately, denoted as HRA_{imp} w/o text attack and HRA_{imp} w/o image attack. Third, we compare our approach with several existing augmentation or transformation strategies, including Random Crop (HRA w Crop), MixUp (HRA w MixUp), Block-wise Augmentation [55] (HRA w BWA), Translation [39] (HRA w TIA) and Rescale [18] (HRA w SIA). Fourth, we replace future-aware momentum with conventional momentum, denoted as (HRA w Mom).

Table VI summarizes all variant results under the image-text retrieval setting, using CLIP_{ViT-B/16} and Flickr30K as the source model and dataset, respectively. The results show that each proposed component contributes positively to attack performance and consistently outperforms corresponding alternatives. These findings further demonstrate the feasibility and importance of considering both the characteristics of UAPs and the optimization path.

F. Visualization

In Figure 6, we showcase some examples of image-text retrieval under the proposed attack. From the figure, it is evident that the proposed method can effectively mislead the target model to return incorrect retrieved data. Additionally, we present some Grad-CAM [56] visualization examples in Figure 7, where it can be seen that the UAPs can significantly change the attention of the target model. These further confirm the effectiveness of the proposed method.

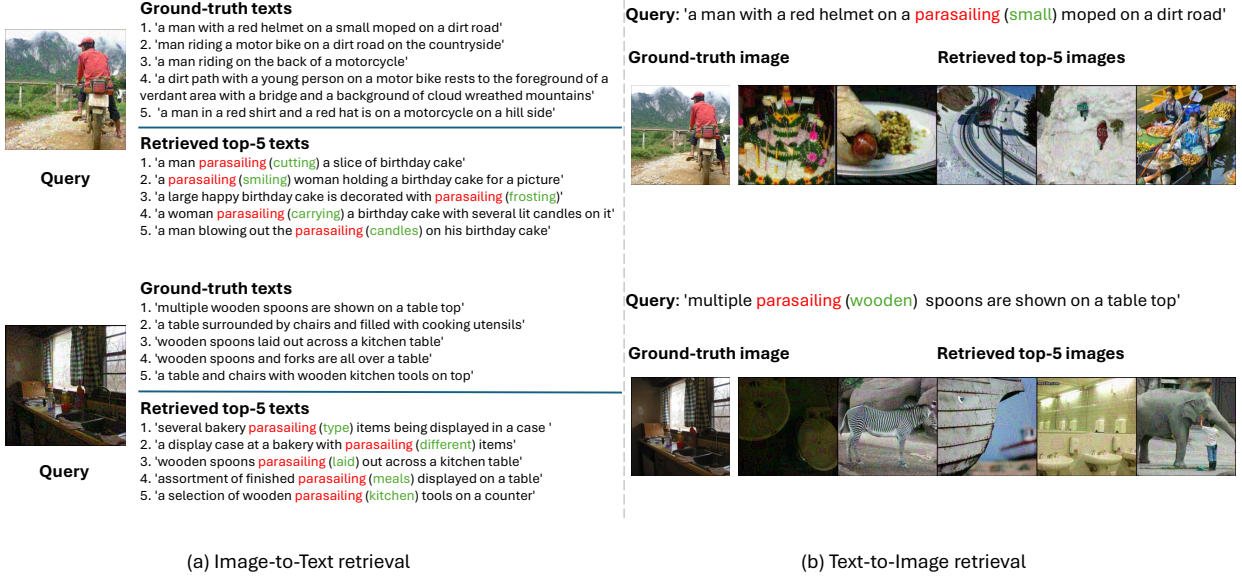


Fig. 6. Examples of top-5 image-text retrieval results. Red words indicate the text UAPs, while green words show the originals.

V. CONCLUSIONS, LIMITATIONS AND FUTURE WORK

A. Conclusions

In this paper, we propose universal multimodal adversarial attacks that aim to efficiently explore the vulnerabilities of VLP models. To enhance adversarial transferability, we introduce a Hierarchical Refinement Attack that jointly explores the sample-agnostic, model-agnostic, and task-agnostic properties of UAPs. Our method performs refinement at both the sample level and the optimization level to produce more transferable perturbations. Extensive experiments across various VLP models, downstream tasks, and datasets demonstrate the effectiveness of the proposed attack.

B. Limitations and Future Work

Despite the significant improvement in universal adversarial transferability, the text attack implemented by inserting a uniform word across different sentences remains perceptible to humans. This is due to the discrete nature of text, even though we restrict the perturbation magnitude. In future work, we aim to develop more imperceptible text-based attacks. Additionally, adversarial transferability is still limited in certain settings, particularly under low perturbation budgets. We plan to further investigate the underlying mechanisms of model perception and explore more effective and transferable universal attack strategies.



Fig. 7. The Grad-CAM visualizations of the original data and the perturbed data.

REFERENCES

[1] A. Radford, J. W. Kim, C. Hallacy, A. Ramesh, G. Goh, S. Agarwal, G. Sastry, A. Askell, P. Mishkin, J. Clark *et al.*, “Learning transferable visual models from natural language supervision,” in *ICML*. PMLR, 2021, pp. 8748–8763.

[2] J. Li, R. Selvaraju, A. Gotmare, S. Joty, C. Xiong, and S. C. H. Hoi, “Align before fuse: vision and language representation learning with momentum distillation,” *NeurIPS*, vol. 34, pp. 9694–9705, 2021.

[3] J. Yang, J. Duan, S. Tran, Y. Xu, S. Chanda, L. Chen, B. Zeng, T. Chilimbi, and J. Huang, “Vision-language pre-training with triple contrastive learning,” in *CVPR*, 2022, pp. 15 671–15 680.

[4] Z. Liu, C. Rodriguez-Opozo, D. Teney, and S. Gould, “Image retrieval on real-life images with pre-trained vision-and-language models,” in *ICCV*, 2021, pp. 2125–2134.

[5] L. Zhou, H. Palangi, L. Zhang, H. Hu, J. Corso, and J. Gao, “Unified vision-language pre-training for image captioning and vqa,” in *AAAI*, vol. 34, no. 07, 2020, pp. 13 041–13 049.

[6] C. Szegedy, W. Zaremba, I. Sutskever, J. Bruna, D. Erhan, I. Goodfellow, and R. Fergus, “Intriguing properties of neural networks,” in *ICLR*, 2014.

[7] P.-F. Zhang and Z. Huang, “A survey on image data perturbations: Challenges, techniques, and impacts,” *TechRxiv preprint*, 2025.

[8] A. Madry, A. Makelov, L. Schmidt, D. Tsipras, and A. Vladu, “Towards deep learning models resistant to adversarial attacks,” in *ICLR*, 2018.

[9] N. Carlini and D. Wagner, “Towards evaluating the robustness of neural networks,” in *SP*, 2017, pp. 39–57.

[10] S. Long, W. Tao, L. Shuo, J. Lei, and J. Zhang, “On the convergence of an adaptive momentum method for adversarial attacks,” in *AAAI*, 2024, pp. 14 132–14 140.

[11] P.-F. Zhang, Z. Huang, X.-S. Xu, and G. Bai, “Effective and robust adversarial training against data and label corruptions,” *IEEE Trans. Multimedia*, vol. 26, pp. 9477–9488, 2024.

[12] P.-F. Zhang, G. Bai, and Z. Huang, “Maa: Meticulous adversarial attack against vision-language pre-trained models,” *arXiv preprint arXiv:2502.08079*, 2025.

[13] P.-F. Zhang, Z. Huang, and X.-S. Xu, “Proactive privacy-preserving learning for retrieval,” in *AAAI*, vol. 35, no. 4, 2021, pp. 3369–3376.

[14] P.-F. Zhang, G. Bai, H. Yin, and Z. Huang, “Proactive privacy-preserving learning for cross-modal retrieval,” *ACM Trans. Inf. Syst.*, vol. 41, no. 2, pp. 1–23, 2023.

[15] P.-F. Zhang, Y. Li, Z. Huang, and H. Yin, “Privacy protection in deep multi-modal retrieval,” in *SIGIR*, 2021, pp. 634–643.

[16] Z. Yin, M. Ye, T. Zhang, J. Wang, H. Liu, J. Chen, T. Wang, and F. Ma, “Vqattack: Transferable adversarial attacks on visual question answering via pre-trained models,” in *AAAI*, 2024, pp. 6755–6763.

[17] J. Zhang, Q. Yi, and J. Sang, “Towards adversarial attack on vision-language pre-training models,” in *ACM MM*, 2022, pp. 5005–5013.

[18] D. Lu, Z. Wang, T. Wang, W. Guan, H. Gao, and F. Zheng, “Set-level guidance attack: boosting adversarial transferability of vision-language pre-training models,” in *ICCV*, 2023, pp. 102–111.

[19] Z. Zhou, S. Hu, M. Li, H. Zhang, Y. Zhang, and H. Jin, “Advclip: downstream-agnostic adversarial examples in multimodal contrastive learning,” in *ACM MM*, 2023, pp. 6311–6320.

[20] P.-F. Zhang, Z. Huang, and G. Bai, “Universal adversarial perturbations for vision-language pre-trained models,” in *SIGIR*, 2024, pp. 862–871.

[21] H. Fang, J. Kong, W. Yu, B. Chen, J. Li, H. Wu, S.-T. Xia, and K. Xu, “One perturbation is enough: On generating universal adversarial perturbations against vision-language pre-training models,” in *ICCV*, 2025, pp. 4090–4100.

[22] P.-F. Zhang, Y. Li, Z. Huang, and X.-S. Xu, “Aggregation-based graph convolutional hashing for unsupervised cross-modal retrieval,” *IEEE Trans. Multimedia*, vol. 24, pp. 466–479, 2021.

[23] P.-F. Zhang, Y. Luo, Z. Huang, X.-S. Xu, and J. Song, “High-order nonlocal hashing for unsupervised cross-modal retrieval,” *World Wide Web*, vol. 24, pp. 563–583, 2021.

[24] P.-F. Zhang, J. Duan, Z. Huang, and H. Yin, “Joint-teaching: learning to refine knowledge for resource-constrained unsupervised cross-modal retrieval,” in *ACM MM*, 2021, pp. 1517–1525.

[25] X. Chen, H. Fang, T.-Y. Lin, R. Vedantam, S. Gupta, P. Dollár, and C. L. Zitnick, “Microsoft coco captions: data collection and evaluation server,” *arXiv preprint arXiv:1504.00325*, 2015.

[26] S. Antol, A. Agrawal, J. Lu, M. Mitchell, D. Batra, C. L. Zitnick, and D. Parikh, “Vqa: visual question answering,” in *ICCV*, 2015, pp. 2425–2433.

[27] N. Xie, F. Lai, D. Doran, and A. Kadav, “Visual entailment: a novel task for fine-grained image understanding,” *arXiv preprint arXiv:1901.06706*, 2019.

[28] Z. Chen, P. Zhang, J. Li, S. Wang, and Z. Huang, “Zero-shot learning by harnessing adversarial samples,” in *ACM MM*, 2023, pp. 4138–4146.

[29] P.-F. Zhang, Y. Cheng, X. Sun, S. Wang, F. Li, L. Zhu, and H. T. Shen, “A step toward world models: A survey on robotic manipulation,” *arXiv preprint arXiv:2511.02097*, 2025.

[30] J. Li, D. Li, C. Xiong, and S. Hoi, “Blip: bootstrapping language-image pre-training for unified vision-language understanding and generation,” in *ICML*. PMLR, 2022, pp. 12 888–12 900.

[31] P. Benz, C. Zhang, A. Karjauv, and I. S. Kweon, “Universal adversarial training with class-wise perturbations,” in *ICME*, 2021, pp. 1–6.

[32] S.-M. Moosavi-Dezfooli, A. Fawzi, O. Fawzi, and P. Frossard, “Universal adversarial perturbations,” in *CVPR*, 2017, pp. 1765–1773.

[33] Y. Li, S. Bai, C. Xie, Z. Liao, X. Shen, and A. Yuille, “Regional homogeneity: Towards learning transferable universal adversarial perturbations against defenses,” in *ECCV*, 2020, pp. 795–813.

[34] X. Liu, Y. Zhong, Y. Zhang, L. Qin, and W. Deng, “Enhancing generalization of universal adversarial perturbation through gradient aggregation,” in *ICCV*, 2023, pp. 4435–4444.

[35] N. Papernot, P. McDaniel, I. Goodfellow, S. Jha, Z. B. Celik, and A. Swami, “Practical black-box attacks against machine learning,” in *ASIA CCS*, 2017, pp. 506–519.

[36] P.-Y. Chen, H. Zhang, Y. Sharma, J. Yi, and C.-J. Hsieh, “Zoo: Zeroth order optimization based black-box attacks to deep neural networks without training substitute models,” in *AISec*, 2017, pp. 15–26.

[37] L. Zhu, T. Wang, J. Li, Z. Zhang, J. Shen, and X. Wang, “Efficient query-based black-box attack against cross-modal hashing retrieval,” *ACM Trans. Inf. Syst.*, vol. 41, no. 3, pp. 1–25, 2023.

[38] Y. Liu, X. Chen, C. Liu, and D. Song, “Delving into transferable adversarial examples and black-box attacks,” in *ICLR*, 2016.

[39] Y. Dong, T. Pang, H. Su, and J. Zhu, “Evading defenses to transferable adversarial examples by translation-invariant attacks,” in *CVPR*, 2019, pp. 4312–4321.

[40] X. Wang, J. Lin, H. Hu, J. Wang, and K. He, “Boosting adversarial transferability through enhanced momentum,” *arXiv preprint arXiv:2103.10609*, 2021.

[41] J. Lin, C. Song, K. He, L. Wang, and J. E. Hopcroft, “Nesterov accelerated gradient and scale invariance for adversarial attacks,” in *ICLR*, 2019.

[42] X. Wang, X. He, J. Wang, and K. He, “Admix: enhancing the transferability of adversarial attacks,” in *ICCV*, 2021, pp. 16 158–16 167.

[43] Y. Xiong, J. Lin, M. Zhang, J. E. Hopcroft, and K. He, “Stochastic variance reduced ensemble adversarial attack for boosting the adversarial transferability,” in *CVPR*, 2022, pp. 14 983–14 992.

[44] B. Chen, J. Yin, S. Chen, B. Chen, and X. Liu, “An adaptive model ensemble adversarial attack for boosting adversarial transferability,” in *ICCV*, 2023, pp. 4489–4498.

[45] N. Inkawich, K. Liang, L. Carin, and Y. Chen, “Transferable perturbations of deep feature distributions,” in *ICLR*, 2019.

[46] Y. Dong, F. Liao, T. Pang, H. Su, J. Zhu, X. Hu, and J. Li, “Boosting adversarial attacks with momentum,” in *CVPR*, 2018, pp. 9185–9193.

[47] A. Kurakin, I. J. Goodfellow, and S. Bengio, “Adversarial examples in the physical world,” *arXiv preprint arXiv:1607.02533*, 2016.

[48] B. A. Plummer, L. Wang, C. M. Cervantes, J. C. Caicedo, J. Hockenmaier, and S. Lazebnik, “Flickr30k entities: collecting region-to-phrase correspondences for richer image-to-sentence models,” in *ICCV*, 2015, pp. 2641–2649.

[49] T.-Y. Lin, M. Maire, S. Belongie, J. Hays, P. Perona, D. Ramanan, P. Dollár, and C. L. Zitnick, “Microsoft coco: common objects in context,” in *ECCV*, 2014, pp. 740–755.

[50] X. Wang and K. He, “Enhancing the transferability of adversarial attacks through variance tuning,” in *CVPR*, 2021, pp. 1924–1933.

[51] L. Yu, P. Poirson, S. Yang, A. C. Berg, and T. L. Berg, “Modeling context in referring expressions,” in *ECCV*. Springer, 2016, pp. 69–85.

[52] A. Dosovitskiy, L. Beyer, A. Kolesnikov, D. Weissenborn, X. Zhai, T. Unterthiner, M. Dehghani, M. Minderer, G. Heigold, S. Gelly *et al.*, “An image is worth 16x16 words: transformers for image recognition at scale,” in *ICLR*, 2020.

[53] K. He, X. Zhang, S. Ren, and J. Sun, “Deep residual learning for image recognition,” in *CVPR*, 2016, pp. 770–778.

[54] D. Wang, W. Yao, T. Jiang, and X. Chen, “Improving transferability of universal adversarial perturbation with feature disruption,” *IEEE Trans. Image Process.*, vol. 33, pp. 722–737, 2024.

[55] X. Wang, Z. Zhang, and J. Zhang, “Structure invariant transformation for better adversarial transferability,” in *ICCV*, 2023, pp. 4607–4619.

[56] R. R. Selvaraju, M. Cogswell, A. Das, R. Vedantam, D. Parikh, and D. Batra, “Grad-cam: visual explanations from deep networks via gradient-based localization,” in *ICCV*, 2017, pp. 618–626.